Author Manuscript

Author Manuscript

Author Manuscript

Author Manuscript

HHS Public Access

Author manuscript

*Dev Dyn*. Author manuscript; available in PMC 2017 October 01.

Published in final edited form as:

*Dev Dyn*. 2016 October ; 245(10): 1029–1042. doi:10.1002/dvdy.24435.

# Development of Myotendinous-like Junctions that Anchor Cardiac Valves Requires Fibromodulin and Lumican

**Loren E. Dupuis**[1], **Lorna Doucette**[1], **A. Kittrell Rice**[1], **Ashton E. Lancaster**[1], **Matthew G. Berger**[1], **Shuki Chakravarti**[2], and **Christine B. Kern**[1]

[1]Department of Regenerative Medicine and Cell Biology, Medical University of South Carolina, Charleston, SC, United States.

[2]Department of Medicine, Johns Hopkins University School of Medicine, Baltimore, MD, United States.

## Abstract

**Background—**There are many patients that exhibit connective tissue related cardiac malformations but do not have mutations in collagen genes. The **S**mall **L**eucine **R**ich **P**roteoglycans (SLRP) fibromodulin (FMOD) and lumican (LUM) bind collagen and regulate fibril assembly in other biological contexts.

**Results—**FMOD deficient mice and double deficient FMOD;LUM mice exhibited anomalies in regions where cardiac valve tissue interdigitates with adjacent muscle for support. Ectopic connective and/or myocardial tissue(s) was associated with the more severe cardiac valve anomalies in FMOD;LUM deficient mice. At postnatal day 0 (P0) there was an increase in the mesenchymal cell number in the regions where valve cusps anchor in FMOD;LUM deficient mice compared to WT. The cardiac valve anomalies correlated with the highest levels of FMOD expression in the heart and also where myotendinous junctions (MTJ) components biglycan, collagen type I alpha 1, and collagen type VI, are also localized.

**Conclusion—**The postnatal assembly of the collagen-rich ECM in regions where cardiac valves anchor, that we have designated ‘myotendinous-like junctions’ (MTLJ) requires the SLRPs FMOD and LUM. Moreover, FMOD and LUM may facilitate mesenchymal cell differentiation in late stages of cardiac valve development.

### Keywords

fibromodulin; lumican; valve; development; myotendinous junction; collagen

## Introduction

The extracellular matrix (ECM) architecture dramatically changes during heart development to provide integrity for cardiac tissues enabling them to perform their function during each cardiac cycle. How the ECM adapts during development to endure biomechanical forces and to maintain unidirectional blood flow in the heart is not well understood. Here we

Correspondence to: Christine B. Kern.

Author Manuscript Author Manuscript Author Manuscript Author Manuscript

investigate, for the first time, the role of the **S**mall **L**eucine **R**ich **P**roteoglycan (SLRP) fibromodulin (FMOD) in cardiac valve development.

Initially endocardial cushions enriched in hyaluronan and the aggregating proteoglycan versican serve as premature valves preventing backflow in the embryonic heart. As development progresses the large, amorphous cushions are sculpted into thin valve cusps that become anchored for support into surrounding tissue. Although basic valve morphology is established prior to birth, the extracellular matrix (ECM) changes dramatically during postnatal development and requires biosynthesis of collagen I-rich fibers to provide strength to the maturing valve cusps (or leaflets). In the adult aortic (AV) and pulmonary valves (PV), the cusps are anchored by integration with the connective tissue of the fibrous annulus; this anchor region interdigitates through specialized ECM with the surrounding myocardial tissue. The fibrous annulus is also referred to as the cardiac skeleton and is organized into continuous overlapping rings of collagen-rich connective tissue at the base of the aortic and pulmonary arteries. In addition, the collagen-rich region provides an attachment for cardiac muscle and insulates the electrical impulses between the atrial and ventricular chambers. The mitral valve (MV) and the tricuspid valve (TV) leaflets anchor within this connective tissue between the left and right atrial-ventricular chambers respectively. In addition these leaflets anchor through chordae tendinae to papillary muscles in their respective ventricles. Based on the differential expression pattern of collagen binding proteins from the family of **S**mall **L**eucine **R**ich **P**roteoglycans (SLRPs), we identified highly specialized regions of collagen I rich tissue at the juncture where cardiac valve cusps or leaflets anchor into adjacent atrial and/or myocardial tissues [1].

The SLRPs instruct collagen fibril growth, organization and extracellular matrix assembly [2-4], binding their leucine rich repeat regions directly to collagen monomers to generate highly specialized connective tissue matrices [5-7]. SLRPs not only have a structural role in regulating the biomaterial properties of collagen-rich ECM but also a signaling role through direct interaction with growth factors [8] and multiple receptors [9-12]. The eighteen different SLRPs are organized into 5 classes based on gene and protein sequence similarity. Although some members of the SLRP family are highly homologous, gene-deletion studies in mice reveal non-overlapping functions of SLRPs [2, 3]. For example, mice deficient in the class II SLRP FMOD have thinner and irregularly fused collagen fibrils in tendons and develop osteoarthritis and weak ligaments [13]. FMOD deficiency also revealed that SLRP mediated collagen assembly is tightly regulated since the protein levels of LUM, a highly homologous class II SLRP, is four-fold higher in the *Fmod*$^{-/-}$ tendon. Interestingly the LUM mRNA level is decreased in *Fmod*$^{-/-}$ tendon, suggesting that the increased amount of LUM protein is due to a reduction of protein degradation rather than an increase in synthesis [13]. Analysis of compound SLRP deficient mice also indicates that multiple SLRPs are required in order to assemble a normal mature collagen-rich matrix in some tendon-like tissues. Deletion of both FMOD and LUM resulted in a more severe tendon phenotype that impacted collagen maturation and ECM architecture, which contributed to joint laxity and impaired tendon integrity [14]. However in other contexts, SLRP compensation is observed. For example, a lack of decorin (DCN) in the cornea is compensated by biglycan (BGN); loss of both DCN and BGN results in a severe eye phenotype, supporting the idea that in some

Author Manuscript Author Manuscript Author Manuscript Author Manuscript

tissues SLRPs can have overlapping functions [15]. A role for SLRPs in vascular homeostasis and disease has been identified for BGN [16, 17] and DCN [18, 19] in regulating elastogenesis and maintaining vascular integrity respectively. There is also indication that some SLRPs mediate pathophysiological stimulation in the heart in response to aortic banding [20] and RV pressure overload [21] as well as an *in vitro* cytokine response [20]. However, the involvement of SLRPs in collagen fiber formation with respect to cardiac valve development has not been experimentally evaluated.

Analysis of the spatiotemporal pattern of SLRPs in the developing murine cardiac valves revealed individualized expression profiles of BGN, DCN, FMOD, and LUM [1]. In fact this study delineated potential differences in the cardiovascular ECM architecture that was not previously appreciated based on the diversity of class I and class II SLRPs expression patterns. For example, FMOD, a class II SLRP, has a discrete region of expression localized to the fibrous annulus region specifically where the semilunar valves anchor into the aortic root. The pattern of FMOD also shows developmental changes in expression. In late fetal stages FMOD is found at the boundaries between undifferentiated mesenchymal cells and myocardial cells and its expression increases dramatically after birth. FMOD expression overlaps with Collagen type I, alpha 1, (Col1a1) at the junction of the valve hinge and the myocardium. In focal anchor regions the class II SLRP LUM also overlaps with FMOD [1]. However the most striking aspect regarding the expression of FMOD and LUM in cardiac valves is the relatively dramatic increase in these SLRPs at birth and into the first month of postnatal life, at regions where valves anchor. The AV and PV anchor into myocardial and arterial tissues and show localized expression of FMOD and LUM. The anchor regions of the atrioventricular valves, the MV and TV, at the base of the ventricles and chordae tendinae are also enriched with FMOD and LUM, albeit at different postnatal time points [1]. Here we test the hypothesis that the maturation of the collagen-I rich ECM in the murine heart requires FMOD and LUM in regions where cardiac valves anchor into myocardial tissue. Since the ECM changes dramatically after birth and includes increases in collagen expression and organization, we speculate that cardiac valve ‘development’ with respect to the roles of FMOD and LUM extends beyond birth and anomalies overlap with high levels of collagen-rich ECM.

## Results

### Phenotypic cardiac screen of *Fmod,* and *Fmod/Lum* double deficient mice revealed a higher penetrance of cardiac valve anomalies than wild type littermate controls

To determine the requirement of FMOD in cardiac valve development we investigated FMOD deficient mice ($Fmod^{-/-}$) for anomalies. Since LUM showed overlapping expression with FMOD and other studies indicate that $Fmod^{-/-}$ and $Lum^{-/-}$ double deficient mice acquire a more severe tendon phenotype than single FMOD or LUM deficient mice [14], we also examined cardiac valves from mice deficient in FMOD that had a reduction in LUM designated: $Fmod^{-/-};Lum^{+/-}$ or were completely deficient in both FMOD and LUM and designated: $Fmod^{-/-};Lum^{-/-}$. FMOD deficient mice ($Fmod^{-/-};Lum^{+/+}$) on a C57BL/6 background breed were indistinguishable from WT littermates as young adults. Mendelian genetic ratios of offspring from double heterozygous intercrosses ($Fmod^{+/-}$; $Lum^{+/-}$ X

Author Manuscript Author Manuscript Author Manuscript Author Manuscript

*Fmod*$^{+/-}$;*Lum*$^{+/-}$) were analyzed at postnatal day 0 (P0; n=106) and in mice aged 1 month (mo) to 4 month (n=150); there was a significant reduction in expected numbers of intercross genotypes. The percent reduced viability of P0 *Fmod*$^{+/-}$; *Lum*$^{+/-}$ X *Fmod*$^{+/-}$;*Lum*$^{+/-}$ offspring was the following: *Fmod*$^{-/-}$;*Lum*$^{+/+}$ (44%), *Fmod*$^{+/+}$;*Lum*$^{-/-}$ (33%), *Fmod*$^{-/-}$;*Lum*$^{+/-}$ (44%) and *Fmod*$^{-/-}$;*Lum*$^{-/-}$ (44%) (**Fig. 1**). The percentage of reduced viability from juvenile and young adult mice (1mo-4 mo) was increased in most of the offspring genotypes compared to P0: *Fmod*$^{-/-}$;*Lum*$^{+/+}$ (77%), *Fmod*$^{+/+}$;*Lum*$^{-/-}$ (62%), *Fmod*$^{-/-}$;*Lum*$^{+/-}$ (12%) and *Fmod*$^{-/-}$;*Lum*$^{-/-}$ (77%). These data represent 34 *Fmod*$^{+/-}$;*Lum*$^{+/-}$ X *Fmod*$^{+/-}$;*Lum*$^{+/-}$ litters. We previously reported a reduction in ventricular lumen area in P0 *Lum*$^{-/-}$ mice that may contribute to unexpected P0 death rates on the C57BL/6 background [22].

In this study we analyzed the cardiac valve phenotypes of P0 and >1mo (late juvenile to young adult; 4 weeks to 4 mo) from offspring of *Fmod*$^{+/-}$;*Lum*$^{+/-}$ X *Fmod*$^{+/-}$;*Lum*$^{+/-}$ intergenetic crosses. Relatively young, 1 mo-4mo, *Fmod*$^{-/-}$;*Lum*$^{+/+}$ mice exhibited a variety of cardiac valve defects with variable penetrance that are summarized in **Table 1**. The cardiac valve anomalies associated with the *Fmod*$^{-/-}$ and *Lum*$^{-/-}$ single mutant mice as well as the combinations of double deficient *Fmod*$^{-/-}$;*Lum*$^{-/-}$ mice included an increase in bicuspid PV and AV valves in *Fmod*$^{-/-}$ that increased in combination with *Lum*$^{-/-}$ i.e. *Fmod*$^{-/-}$;*Lum*$^{-/-}$ mice. Mitral and tricuspid anomalies included myxomatous, i.e. enlarged as well as an increase in leaflet number that was increased in penetrance in double deficient combinations.

## At 1 month, regions that anchor the aortic valves are enriched in FMOD, and other ECM proteins that comprise myotendinous junctions; FMOD deficiency disrupted immunolocalization of MTJ proteins, Biglycan, Collagen type I, alpha 1 and Collagen type VI

Our previously published report indicated that by P0 FMOD is localized in regions where cardiac valves anchor into either arterial or myocardial tissue [1] with very little expression detectable in ventricular muscle (except for early in development). LUM is also present where the aortic (AV) and pulmonary valves (PV) anchor, albeit more prominently expressed at the juncture with arterial tissue [1].

The phenotypic cardiac screen revealed somewhat unexpected anomalies in the wild type (WT) C57BL/6 mice. Previous reports [23, 24] had noted significant phenotypic and sequence differences between C57BL/6J and C57BL/6N strains of ‘normal’ WT mice, however the specific cardiovascular anomalies observed in this study have not been published. Due to the WT anomalies, the ‘n’ number of WT mice was increased to 32 (n=32, 1mo-4mo) mice. In this study ‘Valve Anchor Anomalies’ (**Table 1**) were defined as malformations at the base of the valve cusp or leaflet where the hinge connects with the fibrous annulus, arterial, or myocardial tissue. The frequency of bicuspid aortic and pulmonary valves was also noted (**Table 1**). Examples of ‘Aortic Valve Anomalies’ included valve anchor anomalies, large-myxomatous valve cusps, extra leaflets and abnormal leaflet geometry.

Author Manuscript Author Manuscript Author Manuscript Author Manuscript

In this study we focused on the regions where cardiac valves anchored since these areas exhibited the highest penetrance of anomalies and coincided with the intense immunolocalization of FMOD. The valve anchor region resembles a myotendinous junction (MTJ), albeit this term has not yet been used for the interface of myocardial and connective tissue in the heart. Since a recently published report indicated that FMOD, BGN, Col1a1, and Collagen type VI (Col6) were enriched in MTJ complexes [25], WT and *Fmod*$^{-/-}$ hearts were immunostained for the MTJ ECM proteins FMOD, BGN, Col1a1, and Col6 in 1 month hearts. We hypothesized that loss of FMOD may alter expression of other MTJ ECM proteins in FMOD deficient hearts that exhibited mild to severe cardiac valve anchor anomalies. Histological sections at the level of the aortic valve (AV) (**Fig. 2**) right coronary (RCC) and left coronary cusps (LCC) are shown in a 1 month WT (**Fig. 2A, C, G, I, M, O, S, U)** and a 1 month *Fmod*$^{-/-}$ heart (**Fig. 2B, D, H, J, N, P, T, V)** with a mild cardiac phenotype. In the *Fmod*$^{-/-}$ heart, the RCC anchor region was expanded (**Fig. 2D, J, P, V** white outlines) compared to the WT (**Fig. 2C, I, O, U** white outlines). BGN and Col1a1 expression areas were also increased in the *Fmod*$^{-/-}$ hearts (**Fig. 2J, P** respectively) compared to the WT (**Fig. 2I, O**) and coincided with the increased area of the RCC anchor region in the *Fmod*$^{-/-}$ hearts (**Fig. 2** white outline, **Fig. 2Y**). Col 6 expression was increased in intensity compared to the WT RCC anchor (**Fig.2U, V**). Compared to BGN, Col1a1, and Col6, FMOD exhibited the most intense and restricted area of expression in the AV cardiac valve anchor region (**Fig. 2A**). Positive pixels of immunolocalization for each ECM component and the area of the hinge regions between the WT and *Fmod*$^{-/-}$ hearts were averaged and graphed (Fig. 2Y). The data revealed that the increased amount of staining correlated with the increased area of the hinge anchors in the *Fmod*$^{-/-}$ hearts since the overall percentage of positive pixels per area of hinge was relatively unchanged. Collectively these data revealed that the ECM region rich in MTJ components was expanded in 1 month *Fmod*$^{-/-}$ hearts compared to WT.

## In adult mice, the distal regions of the AV cusps were thinner in the *Fmod*$^{-/-}$ and *Fmod*$^{-/-}$;*Lum*$^{+/-}$ compared to wild type and correlated with reduced BGN, Col1α1 and Col6 immunolocalization

Morphometrics were performed on the proximal hinge, medial hinge and the distal cusp (widest portion) in *Fmod*$^{-/-}$ compared to *Fmod*$^{+/+}$ (**Fig. 1E, F, K, L, Q, R, W, X- Z**) in mice 3 months and older. In the AV the distal portions of the *Fmod*$^{-/-}$ and *Fmod*$^{-/-}$;*Lum*$^{+/-}$ RCC and LCC were significantly smaller than WT (n=8, n=7, n=8 respectively). No significant differences were observed in the proximal hinge or medial hinge regions of AV cusps between genotypes. Scatter plots in **Fig. 2Z** show the range of cusp measurements in the WT (+/+;+/+), *Fmod*$^{-/-}$ (−/−;+/+) and *Fmod*$^{-/-}$;*Lum*$^{+/-}$ (−/−;+/−). The decreased distal cusp width correlated with an apparent reduction in BGN, Col1a1 and Col6 immunolocalization (**Fig. 2E, F, K, L, Q, R, W, X**). A reduction in distal valve cusp size is consistent with aging of aortic valve cusps in mice, presumably due to a decreased ability to biosynthesize collagen matrix [26]. Therefore loss of FMOD during development may have disrupted normal collagen fiber formation in the distal region of RCC and LCC.

Author Manuscript Author Manuscript Author Manuscript Author Manuscript

### ECM proteins that anchor the mitral valve leaflet to the interventricular septum and serve to isolate atrial and ventricular tissues were disrupted in *Fmod*$^{-/-}$ mice at 1 month

Histological sections of the dorsal portion (back) of the *Fmod*$^{+/+}$ and *Fmod*$^{-/-}$ 1 month hearts were examined at the region where the fibrous cap at the top of the interventricular septum (IVS) was contiguous with the atrial septum and leaflet of the MV (**Fig. 3**). In the *Fmod*$^{-/-}$ heart, the disorganization of this region was evident; there was not a clear focal point of separation at the base of the IVS, atrial septum and mitral valve leaflet as in the WT (**Fig. 3A** white box inset, compared to **Fig. 3B** white box inset). Ventricular and atrial muscle tissue was aberrantly located i.e. ectopic, and displaced above the top of the membranous IVS (**Fig.3B, H, N, T** asterisks). In the *Fmod*$^{-/-}$ heart the LA was anchored at a more distal point on the MV leaflet (**Fig 3A** yellow box inset compared to **Fig. 3A, B, G, H, M, N, S, T** yellow box inset). The fibrous ECM of the MV leaflet containing BGN, Col1a1, Col6 was more compacted in the WT at the juncture with the atrial tissue compared to the *Fmod*$^{-/-}$ which gave an expanded and more disorganized appearance (**Fig. 3E, F, K, L, Q, R, W, X,** dashed outline**)**.

### Regions that anchor cardiac valves were disrupted at high penetrance in adult *Fmod*$^{-/-}$ and *Fmod*$^{-/-}$;*Lum*$^{+/-}$ hearts compared to wild type littermates

FMOD localizes to focal regions where cardiac valves anchor into connective tissue adjacent to myocardium and arterial tissue [1]. The *Fmod*$^{-/-}$;*Lum*$^{+/+}$(n=16), *Fmod*$^{+/+}$;*Lum*$^{-/-}$ (n=15), *Fmod*$^{-/-}$;*Lum*$^{+/-}$ (n=13), and *Fmod*$^{-/-}$;*Lum*$^{-/-}$ (n=3) 1.5 month to 5 month hearts exhibited a number of anomalies consistent with abnormal anchoring of cardiac valves. **Figure 4** shows examples of normal PV (**Fig. 4A),** AV (**Fig. 4D**) and MV (**Fig. 4J**) anchor regions while malformations are depicted for *Fmod*$^{-/-}$;*Lum*$^{+/+}$, (**Fig. 4B, E, F, K** solid arrows) *Fmod*$^{-/-}$;*Lum*$^{+/-}$, (**Fig. 4G, H**, solid arrows) and *Fmod*$^{-/-}$;*Lum*$^{-/-}$ (**Fig. 4C, I**, solid arrows). In some hearts the malformed cardiac valve anchor region was accompanied by connective tissue extensions that appeared as extra valve leaflets and resulted in severe anomalies that affected the PV (**Fig. 3C**, open arrow), AV (**Fig. 4E, F, G, H,** open arrows) and MV (**Fig. 4K** open arrow). In the *Fmod*$^{-/-}$;*Lum*$^{+/+}$ juvenile and adult mice the frequency of valve anchor anomalies was 44%, and the *Fmod*$^{-/-}$;*Lum*$^{+/-}$ had a 77% penetrance (**Table 1**). Although there was not a statistically significant number of double deficient adult mice to analyze (*Fmod*$^{-/-}$;*Lum*$^{-/-}$), all 3 exhibited valve anchor malformations (**Fig. 4C, I**). To give a three-dimensional view of these gross valve anomalies, movies were generated of sections from a *Fmod*$^{-/-}$;*Lum*$^{+/+}$ and *Fmod*$^{-/-}$;*Lum*$^{+/-}$ heart (Fig. 3 legend) to compare to WT.

It was noted that a significant percentage *Lum*$^{-/-}$ juvenile and adult hearts (27%, *Fmod*$^{+/+}$;*Lum*$^{-/-}$) contained abnormal valve anchor regions (**Table 1**), however these malformations were different than those observed in the *Fmod*$^{-/-}$;*Lum*$^{+/+}$, *Fmod*$^{-/-}$;*Lum*$^{+/-}$ and *Fmod*$^{-/-}$;*Lum*$^{-/-}$ hearts. Several 1 to 4 month old *Fmod*$^{+/+}$;*Lum*$^{-/-}$ hearts had cartilage-like nodules at the anchor of the RCC (**Fig. 5,** boxes **B, C**). In Movat's pentachrome stained sections, lacunae containing cells shown in boxes (**Fig. 5B, C**) stained green/blue indicative of cartilage (**Fig. 5E, F**). Another AV abnormality from a *Fmod*$^{+/+}$;*Lum*$^{-/-}$ heart is depicted in a ventral section (**Fig. 5H**) and in a more dorsal section (**Fig. 5I**). The lacunae cartilage-like cells are evident and shown magnified in insets (**Fig. 5I**).

Author Manuscript Author Manuscript Author Manuscript Author Manuscript

### Immunohistochemistry of valve anchor anomalies revealed ectopic connective and myocardial tissues in *Fmod*$^{-/-}$;*Lum*$^{+/+}$, *Fmod*$^{-/-}$;*Lum*$^{+/-}$ and *Fmod*$^{-/-}$;*Lum*$^{-/-}$ adult hearts

A subset of the hearts containing valve anchor anomalies in the PV, AV and MV from 1.5 −5 month old mice were immunostained with Col1a1 and muscle markers (either α smooth muscle actin (αSMA) or α sarcomeric actin (α-Sarc)) (**Fig. 6**). The amount of Col1a1-rich tissue was increased in the FMOD and LUM deficient hearts (**Fig. 6B-H,** green, arrows). Additionally, *Fmod*$^{-/-}$;*Lum*$^{+/-}$ and *Fmod*$^{-/-}$;*Lum*$^{-/-}$ hearts had abnormal extensions where Col1a1 was immunolocalized that resembled valve tissue (**Fig. 6F, G, J**, open arrows). Aberrant muscle tissue adjacent to the increased Col1a1-rich regions was also found and is delineated by boxes (**Fig. 6B, C, F, G**). Although the *Fmod*$^{-/-}$;*Lum*$^{+/-}$ and *Fmod*$^{-/-}$;*Lum*$^{-/-}$ hearts exhibited different types of malformations, immunostaining of Col1α1 positive tissue was increased, and α-Sarc positive (myocardial) tissue was ectopically located in regions where cardiac valves are anchored for support.

### At postnatal day 0, *Fmod*$^{-/-}$;*Lum*$^{+/+}$, *Fmod*$^{-/-}$;*Lum*$^{+/-}$ and *Fmod*$^{-/-}$;*Lum*$^{-/-}$ hearts contained an abnormal increase in mesenchymal cells at regions where valves anchor into myocardium

A retrospective developmental study was performed to determine the origins of the adult FMOD deficient cardiac valve related malformations. At postnatal day 0 (P0) we focused on the region where the RCC of the AV anchored and where the anterior leaflet of the MV inserts into the membranous IVS. Immunolocalization of ECM components versican (Vcan) GAGβ and Col1a1 was utilized to define the 'mesenchymal tissue region'. αSarc IHC was performed to label cardiomyocytes (**Fig. 7, 8**). Note that mesenchymal cells are characterized as cells within the GAGβ and/or Col1a1 matrix that are not αSarc positive and do not have cell-cell attachments (like endothelial cells). Cardiac valve anchor anomalies in P0 hearts were examined in FMOD and FMOD/LUM genotypes: *Fmod*$^{-/-}$; Lum$^{+/+}$ (n=6), *Fmod*$^{-/-}$;*Lum*$^{+/-}$ (n=7), and *Fmod*$^{-/-}$;*Lum*$^{-/-}$ (n=4) hearts and compared to WT (*Fmod*$^{+/+}$; *Lum*$^{+/+}$ hearts (n=9)) (**Table 2**). At the RCC anchor an increase in mesenchymal area was observed in 43% of *Fmod*$^{-/-}$;*Lum*$^{+/+}$ hearts compared to 0% in WT. Mesenchymal cell counts revealed a statistically significant increase in the number of mesenchymal cells in the *Fmod*$^{-/-}$; *Lum*$^{+/+}$, *Fmod*$^{-/-}$;*Lum*$^{+/-}$ and *Fmod*$^{-/-}$;*Lum*$^{-/-}$ hearts at the RCC hinge anchor (**Fig. 7M**, $P$ <0.01). There was a statistically significant 35% increase in the number of mesenchymal cells in the *Fmod*$^{-/-}$;*Lum*$^{+/+}$ RCC anchor compared to WT at P0. Further reduction of LUM in the double deficient *Fmod*$^{-/-}$;*Lum*$^{+/-}$ hearts resulted in a phenotypic penetrance of 57% (**Table 2**) with a statistically significant 35% increase in RCC anchor mesenchymal cells. In the *Fmod*$^{-/-}$;*Lum*$^{-/-}$ hearts, there was an increase to 74% of the hearts exhibiting a statistically significant increase of 30% more RCC anchor mesenchymal cells compared to control hearts. The RCC anchor represents one of the highest regions of FMOD expression in P0 WT hearts therefore an emerging phenotype in this area would be consistent with a primary affect of FMOD and LUM deficiency.

In the more posterior region at the juncture of the posterior MV leaflet and IVS, 43% of *Fmod*$^{-/-}$;*Lum*$^{+/+}$ hearts exhibited an increased mesenchymal area, however there was only a trend to an increased cell number, that with an n=7, was not statistically significant. However, LUM deficiency alone resulted in a high phenotypic percentage (86%) with 100%

Author Manuscript Author Manuscript Author Manuscript Author Manuscript

of the *Fmod*$^{-/-}$;*Lum*$^{-/-}$ hearts showing anomalies at the MV/IVS-mesenchymal cap interface. In the posterior region, the increase in mesenchymal cell number was statistically significant in *Fmod*$^{-/-}$;*Lum*$^{+/-}$ and *Fmod*$^{-/-}$;*Lum*$^{-/-}$ hearts with a similar number of increased cells (**Fig. 8M**, $P < 0.01$); a higher n number from each genotype would be required to determine the specific contribution of FMOD and LUM deficiency to the increased mesenchymal cells in this region. Immunolocalization of both Vcan GAGβ and Col1a1 was outlined in the posterior regions where the anterior leaflet of the MV anchored into the IVS to highlight the mesenchymal cell regions measured in this analysis (**Fig. 8A-C, G-L**). The ECM in the MV/IVS region is particularly rich in FMOD during development [1]. Therefore the malformations at the MV/IVS-mesenchymal cap, as well as the anomalies associated with additional MV leaflets, are likely a primary effect of FMOD and/or LUM deficiency. Although postnatal cardiac valve anomalies are described, a thorough analysis of embryonic time points beginning at embryonic day 13.5 (E13.5) to E17.5 was performed. Table 2 shows the lack of phenotypic penetrance of E17.5 hearts examined for cardiac valve anchor related anomalies. Therefore, the cardiac phenotype in the *Fmod* and *Lum* deficient mice was evident at birth and appeared to increase in severity in the first month of life as mesenchymal and myocardial cells terminally differentiate and as more collagen-rich ECM is assembled.

## Discussion

This study was the first to investigate the role of FMOD in cardiac valve development to determine if loss of FMOD affected Col1a1-rich connective tissue in the murine heart. The cardiac anomalies in the FMOD deficient mice corresponded to areas where we previously reported concentrated expression of FMOD. One of the surprising aspects of the cardiac valve-related phenotype was that the onset of notable anomalies was at birth; embryonic hearts from *Fmod* and *Fmod;Lum* deficient mice were thoroughly examined for cardiac valve anomalies however there was no phenotype observed at these earlier time points. Collectively, postnatal regions where anomalies developed were in collagen-rich ECM that anchor cardiac valves into myocardial tissue are similar to MTJs that bridge the connection between tendons and skeletal muscle. The MTJ is characterized as a complex, specialized region located at the muscle-tendon interface that functions as a primary site of force transmission [27]. The structure of the MTJ involves an alignment of protein complexes from the muscle cells' basal lamina to the collagen matrix on the tendinous side of the MTJ. Recently, a combination of laser capture microscopy (LCM) and liquid chromatography tandem mass spectrometry (LCMS/MS) was used to profile proteins that comprise the MTJ of mouse skeletal muscles. FMOD emerged as a highly enriched component of the connective tissue of the MTJ with one of the highest Mascot scores of all the MTJ ECM factors identified. Although not exclusively expressed in the MTJ, FMOD is more prominently expressed in the MTJ compared to the tendon proper [25]. In the developing heart, FMOD is predominantly expressed in regions where tendinous valve tissue anchors into surrounding muscle. Consistent with the role of the MTJ at the muscle tendon interface, the valve anchor regions also withstand and transmit significant biomechanical force from the rapidly moving valve cusps. Moreover, BGN, Col1a1 and Col6, proteins enriched in MTJ of the skeletal muscle, were also localized in cardiac regions where FMOD was highly

Author Manuscript Author Manuscript Author Manuscript Author Manuscript

expressed and that were disrupted in the FMOD deficient hearts. Therefore we have designated the region where connective tissue extensions of the cardiac valves interdigitate into surrounding myocardial tissue a ‘myotendinous-like junction’ (MTLJ). This murine cardiac MTLJ contains highly specialized collagen I rich ECM that is disrupted in a high percentage of FMOD deficient hearts. FMOD expression is restricted to focal regions where the PV and AV cusps anchor. However, in the dorsal aspect of the heart the FMOD rich connective tissue is more extensive and serves to isolate atrial from ventricular myocardium and to anchor the TV and MV leaflets. The malformations in the FMOD deficient and combination FMOD/LUM mutant mice suggest that the murine heart requires these SLRPs to assemble highly specialized Col1a1 containing fibers in what we have designated the MTLJ regions of the murine heart.

The formation of the MTJ occurs in stages and initiates where undifferentiated tenoblasts and myoblasts are in close proximity. In the heart, FMOD is expressed at the interface of undifferentiated mesenchyme (fibroblasts) and myocardial cells (smooth muscle cells) at birth. These mesenchymal cells differentiate postnatally coincident with a dramatic increase in collagen and FMOD deposition. Eventually the mesenchymal cells within the MTLJ complex where PV and AV valves anchor will be continuous with the connective tissue of the mature annulus fibrosis [28]. In the FMOD deficient and FMOD/LUM double deficient hearts there was an apparent increase in the number of undifferentiated mesenchymal cells in MTLJ-valve anchor regions. In young adult FMOD deficient and FMOD/LUM double mutant hearts we observed ectopic tissue at the malformed MTLJ regions. This ectopic tissue is a characteristic of disrupted MTJ complexes in other contexts [27]. In the disrupted skeletal muscle MTJ, muscle cells migrate to ectopic regions in the absence of tendon precursors; in normal MTJ development apoptosis occurs and eliminates myotubes that are not anchored into MTJ ECM. One interpretation of the severe FMOD deficient phenotypes is that FMOD is required to control the number of myocardial and fibroblast cells through apoptosis and/or to promote terminal differentiation. It is well established that postnatal terminal cardiomyocyte differentiation in the heart coordinates with extensive collagen biosynthesis. We speculate that FMOD is required to generate a specialized ECM boundary that we refer to as the MTLJ which facilitates differentiation of cardiomyocytes and fibroblasts and provides structural integrity and anchoring for cardiac valves.

Since the MTJ serves as a point of mechanotransduction in other tissues, further evaluation of the FMOD deficient cardiac phenotypes may elucidate its signaling role during mechanotransduction in regions of ECM where cardiac valves anchor. Several reports indicate that FMOD is upregulated in response to mechanical stimulation [29-31]; however, the signaling pathways involved have not been elucidated. The addition of FMOD via polymer based transfection results in increased healing of tendons compared to other factors (LUM, PDGF). It is well established that the class I SLRP decorin interacts with TGFβ to influence myoblast proliferation and differentiation [32, 33]. In human osteosarcoma cells LUM is an endogenous inhibitor of TGF-β2 activity [34]. We showed that FMOD/LUM deficiency in the murine heart resulted in focal regions of the MTLJ that also exhibited an apparent increase in BGN. In other contexts BGN also binds and sequesters TGFβ in the developing skeletal muscle and bone [35, 36]. Although the ECM architecture mirrors the biomechanical forces it endures, how mechanotransduction is involved to specialize

Author Manuscript Author Manuscript Author Manuscript Author Manuscript

biosynthesis of collagen-rich matrices is a poorly understood aspect of ECM biology. Studies here demonstrated that FMOD is likely to play a role in both the structural integrity of the ECM that anchors valves as well as to signal differentiation of connective and myocardial cell precursors. While this study was the first to elucidate a potential role for FMOD related to cardiac valves, the mechanism by which FMOD and/or FMOD /LUM deficiency impacts cell behavior and signaling during formation of the MTLJ warrants further study.

Many patients exhibit cardiac malformations or defects related to collagen synthesis and turnover but do not have mutations in collagen genes. To date there are very few human genetic mutations that are linked to SLRP genes. The only collagen-related disorders attributed to mutations in SLRP genes within the human populations are primarily associated with corneal pathologies [37-41]. Note that the double deficient $Fmod^{-/-};Lum^{-/-}$ mice had a completely penetrant bicuspid AV phenotype and the PV also had an increase in bicuspid malformations. Our recent work on the $Adamts5^{-/-}$ mice that also had a reduction in collagen fiber formation i.e. ECM transition also exhibited a significant penetrance of bicuspid PV and AV on the $Smad2^{+/-}$ background [42]. The MTLJ shares similarities with developmental processes where cusp excavation occurs that, when delayed, results in bicuspid valve formation. Data here further validate that ECM transition that impact collagen formation likely contributes to bicuspid malformations in mice; the relevance to this prevalent malformation in the human population is yet to be explored. Findings in this study suggest that mutations that may reduce FMOD and/or LUM in the heart may disrupt localized regions where the Col1α1 rich matrix interdigitates with myocardial tissue to anchor the cardiac valves, processes also relevant to bicuspid anomalies in the AV and PV. We speculate that in these regions the specialized collagen-rich tissue requires FMOD for the appropriate differentiation of mesenchymal cells, connective tissue integrity and mechanotransduction within MTLJ regions of the murine heart.

## Experimental Procedures

### Mice

All experiments using mice were done under approved IACUC protocols of the Medical University of South Carolina.

### Histology and Immunohistochemistry

Standard histological procedures were used [43]. Murine tissue used was either fixed in 4% Paraformaldehyde and paired with citric acid antigen unmasking (H-3300, Vector Laboratories, Burlingame, CA), or fixed in Amsterdam fixative (35% methanol, 35% acetone, 5% acetic acid). The fibromodulin and biglycan antibodies used were a gift from Dr. L. Fisher, at the National Institute of Health. An antibody to Col1a1 against mouse was purchased from mdbioproducts (203002) and Col6 against rabbit was purchased from Rockland Antibodies (600-401-108). The Gagβ Vcan antibody was a gift from Dr. S. Hoffman and used to identify versican. Antibodies were purchased from Sigma to α-sarcomeric actin (A2172) to identify myocardial cells and to α-smooth muscle actin (A5228) to identify smooth muscle cells. Fluor-conjugated secondary antibodies were

Author Manuscript Author Manuscript Author Manuscript Author Manuscript

purchased from Jackson ImmunoResearch (West Grove, PA). Nuclei were labeled with propidium iodide from Sigma (P4864). The Leica TCS SP5 AOBS Confocal Microscope System (Leica Microsystems Inc., Exton, PA) was used to obtain images. Modified Movat's pentachrome staining was performed as previously described [44].

### Cardiac Valve Morphometrics

Measurements were collected to quantify observed differences in cusp width at the proximal, medial and distal portions of the valve cusp. Eight measurements were taken at each location from histological sections at the widest part of the cusp through a depth of at least 60μm per sample. An Olympus BX40 microscope (Olympus Corporation, Center Valley, PA) with DP2-BSW (v1.4, build 2743) software was used to obtain measurements. A minimum of seven animals was used for each genotype investigated. Student's t-test (2 tailed, type 2), followed by Anova was utilized to determine statistical significance ($P < 0.05$).

### Mesenchymal cell counts

Nuclei were counted in the mesenchymal regions of the right coronary cusp (RCC) from the aortic valve and at the juncture of the interventricular septum (IVS) and atrial septum, at a depth where both the tricuspid and mitral valve were observed at P0. A minimum of two histological sections that represented a depth of at least 10μm were utilized. Mesenchymal regions were defined as areas negative for α sarcomeric actin at the base of the RCC or at the juncture of the atrial septum and interventricular septum; in addition, ECM markers versican GAG β and or Col1α1 were used to identify mesenchymal cells. A minimum of four animals was used for each genotype investigated. ‘Phenotypic’ in the table refers to hearts that were 10% above the WT highest count range. Student's t-test was used when comparing two groups. ANOVA was utilized to determine statistical significance when comparing more than two groups and the *P*-values were corrected using Scheffe's adjustment for multiple comparisons.

## Supplementary Material

Refer to Web version on PubMed Central for supplementary material.

## Acknowledgements

The authors would like to thank Dr. Marian Young for providing the FMOD deficient mice and for sharing her expertise in SLRP biology. This work was supported by NIH RO1 HL121382 (CBK), NIH-NGMS P30 GM103342.

## Abbreviations

| | |
|---|---|
| **ECM** | extracellular matrix |
| **fmod** | fibromodulin |
| **lum** | lumican |
| **MTJ** | myotendinous junction |

Author Manuscript Author Manuscript Author Manuscript Author Manuscript

| | |
|---|---|
| **MTLJ** | myotendinous-like junction |
| **PV** | pulmonary valve |
| **AV** | aortic valve |
| **MV** | mitral valve |
| **IVS** | interventricular septum |
| **AS** | atrial septum |
| **Col1a1** | collagen type I alpha 1 |
| **BGN** | biglycan |
| **Col6** | collagen type 6 |

## References


1. Dupuis LE, Kern CB. Small leucine-rich proteoglycans exhibit unique spatiotemporal expression profiles during cardiac valve development. Dev Dyn. 2014; 243(4):601–11. [PubMed: 24272803]
2. Kalamajski S, Oldberg A. The role of small leucine-rich proteoglycans in collagen fibrillogenesis. Matrix Biol. 2010; 29(4):248–53. [PubMed: 20080181]
3. Ameye L, Young MF. Mice deficient in small leucine-rich proteoglycans: novel in vivo models for osteoporosis, osteoarthritis, Ehlers-Danlos syndrome, muscular dystrophy, and corneal diseases. Glycobiology. 2002; 12(9):107R–16R.
4. Chen S, Birk DE. The regulatory roles of small leucine-rich proteoglycans in extracellular matrix assembly. FEBS J. 2013; 280(10):2120–37. [PubMed: 23331954]
5. Chakravarti S, et al. Collagen fibril assembly during postnatal development and dysfunctional regulation in the lumican-deficient murine cornea. Dev Dyn. 2006; 235(9):2493–506. [PubMed: 16786597]
6. Chen S, et al. Fibromodulin regulates collagen fibrillogenesis during peripheral corneal development. Dev Dyn. 2010; 239(3):844–54. [PubMed: 20108350]
7. Ezura Y, et al. Differential expression of lumican and fibromodulin regulate collagen fibrillogenesis in developing mouse tendons. J Cell Biol. 2000; 151(4):779–88. [PubMed: 11076963]
8. Iozzo RV, Schaefer L. Proteoglycans in health and disease: novel regulatory signaling mechanisms evoked by the small leucine-rich proteoglycans. FEBS J. 2010; 277(19):3864–75. [PubMed: 20840584]
9. Santra M, Reed CC, Iozzo RV. Decorin binds to a narrow region of the epidermal growth factor (EGF) receptor, partially overlapping but distinct from the EGF-binding epitope. J Biol Chem. 2002; 277(38):35671–81. [PubMed: 12105206]
10. Goldoni S, Iozzo RV. Tumor microenvironment: Modulation by decorin and related molecules harboring leucine-rich tandem motifs. Int J Cancer. 2008; 123(11):2473–9. [PubMed: 18798267]
11. Schonherr E, et al. Decorin, a novel player in the insulin-like growth factor system. J Biol Chem. 2005; 280(16):15767–72. [PubMed: 15701628]
12. Schaefer L, et al. Decorin-mediated regulation of fibrillin-1 in the kidney involves the insulin-like growth factor-I receptor and Mammalian target of rapamycin. Am J Pathol. 2007; 170(1):301–15. [PubMed: 17200203]
13. Svensson L, et al. Fibromodulin-null mice have abnormal collagen fibrils, tissue organization, and altered lumican deposition in tendon. J Biol Chem. 1999; 274(14):9636–47. [PubMed: 10092650]
14. Jepsen KJ, et al. A syndrome of joint laxity and impaired tendon integrity in lumican- and fibromodulin-deficient mice. J Biol Chem. 2002; 277(38):35532–40. [PubMed: 12089156]

Author Manuscript Author Manuscript Author Manuscript Author Manuscript

15. Zhang G, et al. Genetic evidence for the coordinated regulation of collagen fibrillogenesis in the cornea by decorin and biglycan. J Biol Chem. 2009; 284(13):8888–97. [PubMed: 19136671]
16. Hwang JY, et al. Retrovirally mediated overexpression of glycosaminoglycan- deficient biglycan in arterial smooth muscle cells induces tropoelastin synthesis and elastic fiber formation in vitro and in neointimae after vascular injury. Am J Pathol. 2008; 173(6):1919–28. [PubMed: 18988796]
17. Schaefer L, et al. Regulation of fibrillin-1 by biglycan and decorin is important for tissue preservation in the kidney during pressure-induced injury. Am J Pathol. 2004; 165(2):383–96. [PubMed: 15277214]
18. Reinboth B, et al. Molecular interactions of biglycan and decorin with elastic fiber components: biglycan forms a ternary complex with tropoelastin and microfibril-associated glycoprotein 1. J Biol Chem. 2002; 277(6):3950–7. [PubMed: 11723132]
19. Trask BC, et al. The microfibrillar proteins MAGP-1 and fibrillin-1 form a ternary complex with the chondroitin sulfate proteoglycan decorin. Mol Biol Cell. 2000; 11(5):1499–507. [PubMed: 10793130]
20. Engebretsen KV, et al. Lumican is increased in experimental and clinical heart failure, and its production by cardiac fibroblasts is induced by mechanical and proinflammatory stimuli. FEBS J. 2013; 280(10):2382–98. [PubMed: 23480731]
21. Waehre A, et al. Chemokines regulate small leucine-rich proteoglycans in the extracellular matrix of the pressure-overloaded right ventricle. J Appl Physiol (1985). 2012; 112(8):1372–82. [PubMed: 22345433]
22. Dupuis LE, et al. Lumican deficiency results in cardiomyocyte hypertrophy with altered collagen assembly. J Mol Cell Cardiol. 2015; 84:70–80. [PubMed: 25886697]
23. Simon MM, et al. A comparative phenotypic and genomic analysis of C57BL/6 and C57BL/6N mouse strains. Genome Biology. 2013; 14(R82):1–22.
24. Serpi R, et al. Inbred wild type mouse strains have distinct spontaneous morphological phenotypes. Histol Histopathol. 2013; 28(1):79–88. [PubMed: 23233061]
25. Can T, et al. Proteomic analysis of laser capture microscopy purified myotendinous junction regions from muscle sections. Proteome Sci. 2014; 12:25. [PubMed: 25071420]
26. Krishnamurthy VK, et al. Maladaptive matrix remodeling and regional biomechanical dysfunction in a mouse model of aortic valve disease. Matrix Biol. 2012
27. Charvet B, Ruggiero F, Le Guellec D. The development of the myotendinous junction. A review. Muscles Ligaments Tendons J. 2012; 2(2):53–63. [PubMed: 23738275]
28. Kruithof BP, Krawitz SA, Gaussin V. Atrioventricular valve development during late embryonic and postnatal stages involves condensation and extracellular matrix remodeling. Dev Biol. 2007; 302(1):208–17. [PubMed: 17054936]
29. Popov C, et al. Mechanical stimulation of human tendon stem/progenitor cells results in upregulation of matrix proteins, integrins and MMPs, and activation of p38 and ERK1/2 kinases. BMC Mol Biol. 2015; 16:6. [PubMed: 25880261]
30. Wang P, Yang L, Hsieh AH. Nucleus pulposus cell response to confined and unconfined compression implicates mechanoregulation by fluid shear stress. Ann Biomed Eng. 2011; 39(3): 1101–11. [PubMed: 21132369]
31. Omlor GW, et al. Changes in gene expression and protein distribution at different stages of mechanically induced disc degeneration--an in vivo study on the New Zealand white rabbit. J Orthop Res. 2006; 24(3):385–92. [PubMed: 16479572]
32. Miura T, et al. Decorin binds myostatin and modulates its activity to muscle cells. Biochem Biophys Res Commun. 2006; 340(2):675–80. [PubMed: 16380093]
33. Kishioka Y, et al. Decorin enhances the proliferation and differentiation of myogenic cells through suppressing myostatin activity. J Cell Physiol. 2008; 215(3):856–67. [PubMed: 18163379]
34. Nikitovic D, et al. Lumican regulates osteosarcoma cell adhesion by modulating TGFbeta2 activity. Int J Biochem Cell Biol. 2011; 43(6):928–35. [PubMed: 21421073]
35. Brandan E, Cabello-Verrugio C, Vial C. Novel regulatory mechanisms for the proteoglycans decorin and biglycan during muscle formation and muscular dystrophy. Matrix Biol. 2008; 27(8): 700–8. [PubMed: 18694824]

Author Manuscript Author Manuscript Author Manuscript Author Manuscript

36. Brandan E, et al. The low density lipoprotein receptor-related protein functions as an endocytic receptor for decorin. J Biol Chem. 2006; 281(42):31562–71. [PubMed: 16936287]
37. Bredrup C, et al. Congenital stromal dystrophy of the cornea caused by a mutation in the decorin gene. Invest Ophthalmol Vis Sci. 2005; 46(2):420–6. [PubMed: 15671264]
38. Majava M, et al. Novel mutations in the small leucine-rich repeat protein/proteoglycan (SLRP) genes in high myopia. Hum Mutat. 2007; 28(4):336–44. [PubMed: 17117407]
39. Wang IJ, et al. The association of single nucleotide polymorphisms in the 5′-regulatory region of the lumican gene with susceptibility to high myopia in Taiwan. Mol Vis. 2006; 12:852–7. [PubMed: 16902402]
40. Chen ZT, et al. The association of haplotype at the lumican gene with high myopia susceptibility in Taiwanese patients. Ophthalmology. 2009; 116(10):1920–7. [PubMed: 19616852]
41. Pellegata NS, et al. Mutations in KERA, encoding keratocan, cause cornea plana. Nat Genet. 2000; 25(1):91–5. [PubMed: 10802664]
42. Dupuis LE, et al. Insufficient versican cleavage and Smad2 phosphorylation results in bicuspid aortic and pulmonary valves. J Mol Cell Cardiol. 2013; 60:50–9. [PubMed: 23531444]
43. Kern CB, et al. Versican proteolysis mediates myocardial regression during outflow tract development. Dev Dyn. 2007; 236(3):671–83. [PubMed: 17226818]
44. Kern CB, et al. Reduced versican cleavage due to Adamts9 haploinsufficiency is associated with cardiac and aortic anomalies. Matrix Biol. 2010; 29(4):304–16. [PubMed: 20096780]

Author Manuscript Author Manuscript Author Manuscript Author Manuscript

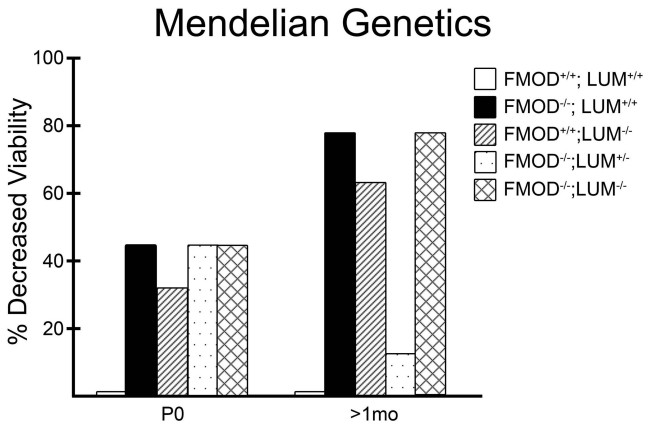


| P0 | Genotype (FMOD) (LUM) | Number Expected | Number Observed | % Decreased Viability |
|---|---|---|---|---|
| | (+/+) (+/+) | 9 | 9 | 0.0% |
| | (+/-) (+/+) | 18 | 18 | 0.0% |
| | (+/+) (+/-) | 18 | 15 | 17% |
| | (+/-) (+/-) | 36 | 29 | 20% |
| | (-/-) (+/+) | 9 | 5 | **44%** |
| | (+/+) (-/-) | 9 | 6 | **33%** |
| | (-/-) (+/-) | 18 | 10 | **44%** |
| | (+/-) (-/-) | 18 | 9 | **50%** |
| | (-/-) (-/-) | 9 | 5 | **44%** |
| | Total | 144 | 106 | 26% |
| | | | | $x^2$=0.07 |

| >1mo | Genotype (FMOD) (LUM) | Number Expected | Number Observed | % Decreased Viability |
|---|---|---|---|---|
| | (+/+) (+/+) | 13 | 13 | 0.0% |
| | (+/-) (+/+) | 26 | 25 | 3.8% |
| | (+/+) (+/-) | 26 | 20 | 23% |
| | (+/-) (+/-) | 52 | 53 | -1.9% |
| | (-/-) (+/+) | 13 | 3 | **77%** |
| | (+/+) (-/-) | 13 | 5 | **62%** |
| | (-/-) (+/-) | 26 | 23 | 12% |
| | (+/-) (-/-) | 26 | 5 | **81%** |
| | (-/-) (-/-) | 13 | 3 | **77%** |
| | Total | 208 | 150 | **72%** |
| | | | | $x^2$=4.8x10$^{-6}$ |

**Fig. 1. Decreased viability of FMOD and LUM deficient mice was observed in offspring from *Fmod*$^{+/-}$;*Lum*$^{+/-}$ X *Fmod*$^{+/-}$;*Lum*$^{+/-}$ intercrosses**

Graphs display percent decreased viability at P0 and >1mo from 34 litters generated from *Fmod*$^{+/-}$;*Lum*$^{+/-}$ X *Fmod*$^{+/-}$;*Lum*$^{+/-}$. The number of expected animals versus the number of observed animals is displayed for each genotype. Bold numbers highlight genotypes that exhibited > 30% death. At P0, 106 mice were analyzed and showed deviation from Mendelian ratios ($x^2$= 0.07). At >1mo, 150 offspring were analyzed and revealed a deviation from Mendelian ratios ($x^2$= 4.8×10$^{-6}$).

Author Manuscript Author Manuscript Author Manuscript Author Manuscript

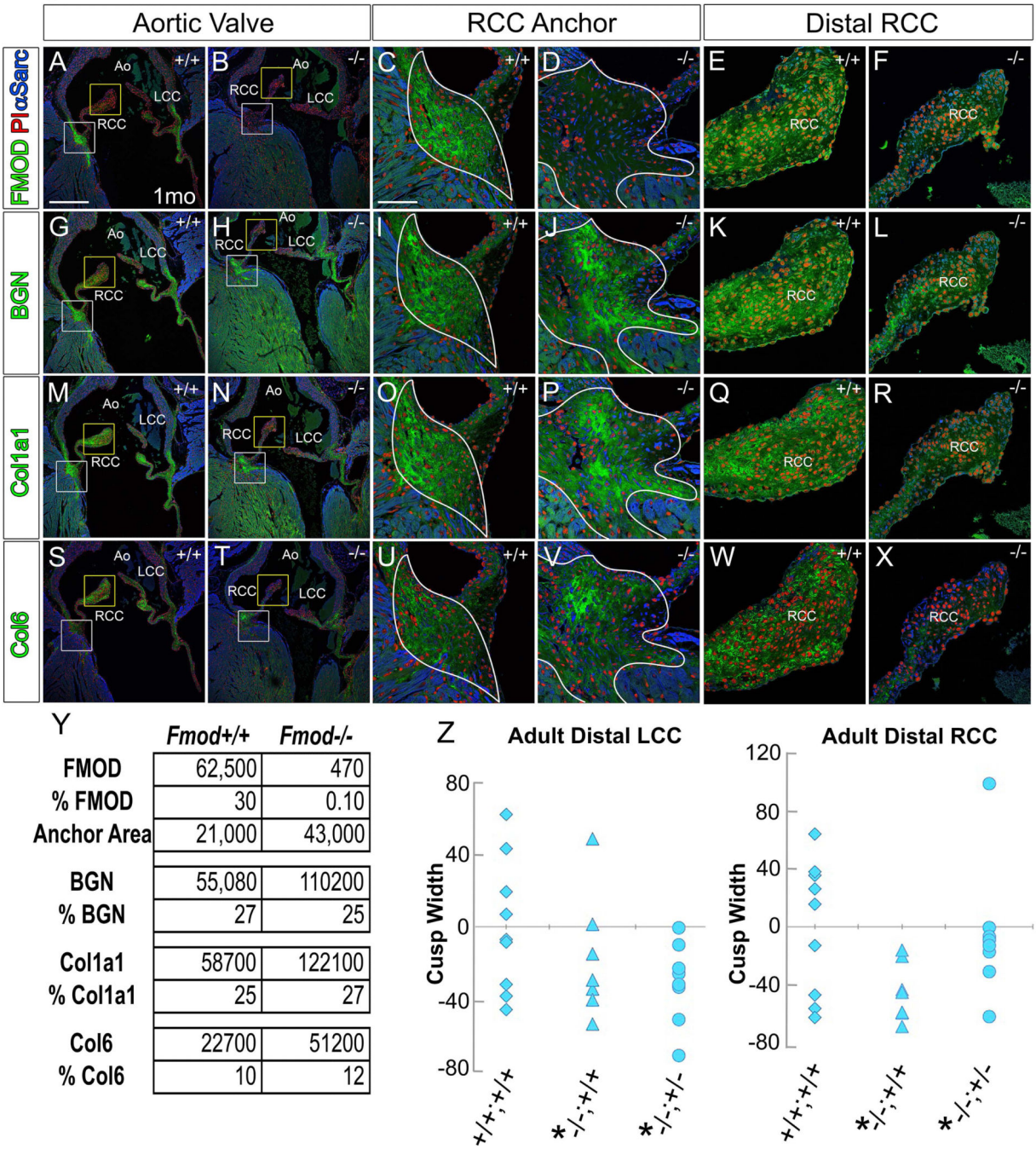


**Fig. 2. Immunostaining of myotendinous junction components biglycan, fibromodulin, Collagen, type I, alpha1 and Collagen 6 was expanded in 1 month *Fmod*$^{-/-}$ hearts where aortic valve cusps anchor compared to wild type**

Immunolocalization of fibromodulin (FMOD, green, A-F), biglycan (BGN, green, G-L), collagen, type I, alpha1 (Col1a1, green, M-R), and collagen 6 (Col6, green, S-X) in *Fmod*$^{+/+}$ (A, C, E, G, I, K, M, O, Q, S, U, W) and *Fmod*$^{-/-}$ (B, D, F, H, J, L, N, P, R, T, V, X). White boxes in A, B, G, H, M, N, S, T are magnified in panels C, D, I, J, O, P, U, V respectively and show the right coronary cusp (RCC) anchor. The yellow boxes in A, B, G, H, M, N, S, T are magnified in panels E, F, K, L, Q, R, W, X respectively and show the distal RCC. White

Author Manuscript Author Manuscript Author Manuscript Author Manuscript

outline (C, D, I, J, O, P, U, V) –collagen-rich region where the RCC anchors. Red-propidium iodide (PI); blue- α-sarcomeric actin (αSarc); LCC- left coronary cusp; Ao-aorta. Scale bars: A= 400μm applies to B, G, H, M, N, S, T; C= 50μm applies to D-F, I-L, O-R, U-X. Table in Y denotes the average area of the anchor region and positive pixels of each ECM components in 1 mo *Fmod*$^{-/-}$ hearts. Scatterplots in Z represent the average width of the RCC and LCC respectively of mice 3 months and older. Each symbol represents the average of one heart through 60μm. *-statistical significance $P < 0.05$.

Author Manuscript
Author Manuscript
Author Manuscript
Author Manuscript



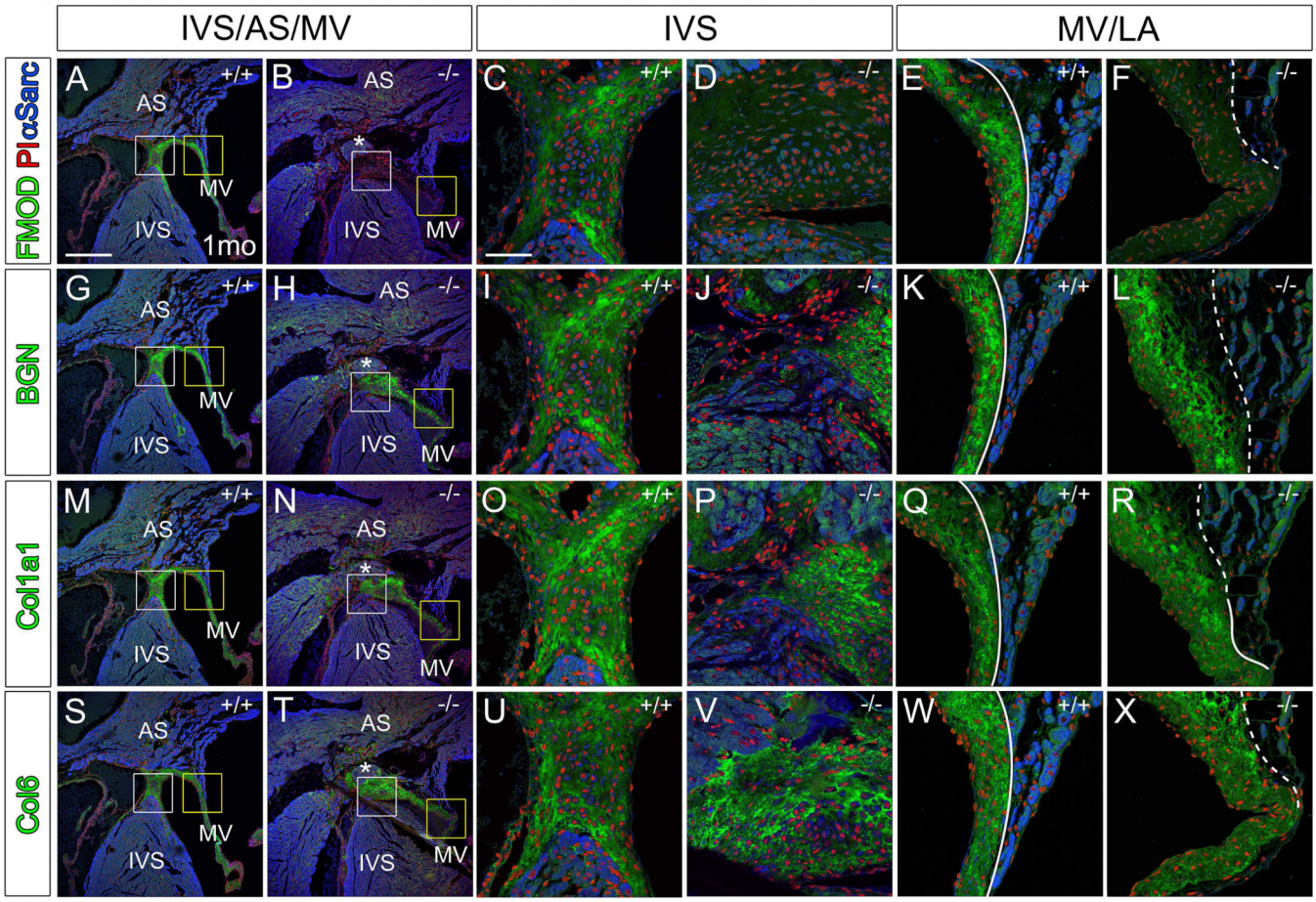


**Fig. 3. Immunolocalization of myotendinous junction proteins BGN, FMOD, Col1a1 and Col6 was expanded in 1 month *Fmod*$^{-/-}$ hearts at the mesenchymal cap of the interventricular septum where the mitral valve leaflet anchors**

Immunolocalization of FMOD (green, A-F), BGN (green, G-L), Col1a1 (green, M-R), and Col6 (green, S-X) in *Fmod*$^{+/+}$ (A, C, E, G, I, K, M, O, Q, S, U, W) and *Fmod*$^{-/-}$ (B, D, F, H, J, L, N, P, R, T, V, X) mitral leaflet attachments. White boxes in A, B, G, H, M, N, S, T are magnified in panels C, D, I, J, O, P, U, V respectively. Yellow boxes in A, B, G, H, M, N, S, T are magnified and shown in E, F, K, L, Q, R, W, X respectively. Red- propidium iodide (PI); blue- α-sarcomeric actin (αSarc); IVS-interventricular septum; AS- atrial septum; MV-mitral valve; LA- left atrium; solid lines- distinct separation of MV and LA; dashed lines-diffuse attachment of left atrial to MV. Scale bars: A= 400μm applies to B, G, H, M, N, S, T; C= 50μm applies to D-F, I-L, O-R, U-X.

Author Manuscript Author Manuscript Author Manuscript Author Manuscript

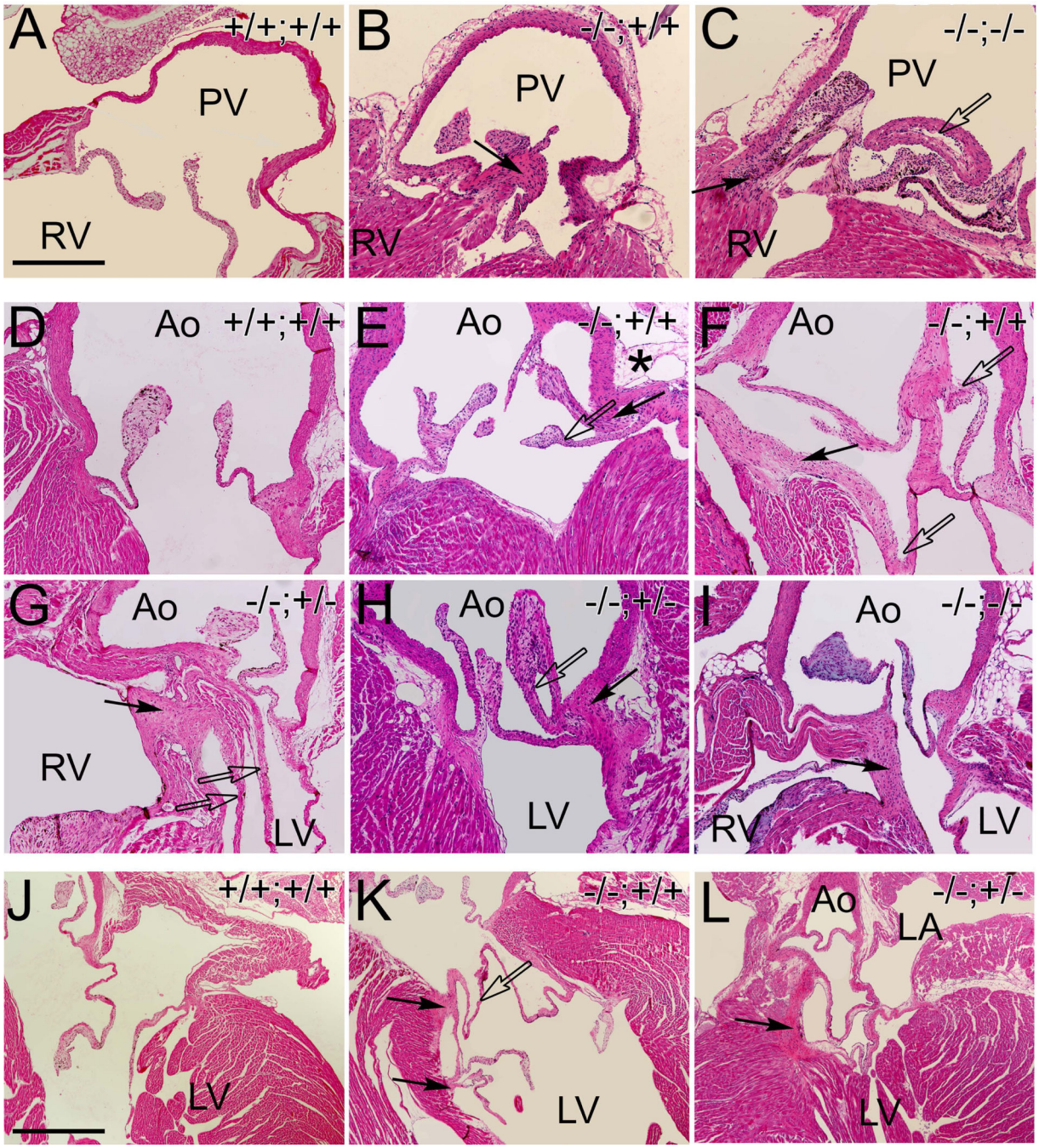


**Fig. 4. Pulmonary, aortic and mitral valves in the *Fmod*$^{-/-}$;*Lum*$^{+/+}$, *Fmod*$^{-/-}$;*Lum*$^{+/-}$ and *Fmod*$^{-/-}$;*Lum*$^{-/-}$ adult hearts exhibited abnormal cusp attachment and ectopic tissue**

Hematoxylin and eosin stained sections from the pulmonary valve (A-C) aortic valve (D-I) and mitral valve (J-L) of *Fmod*$^{+/+}$;*Lum*$^{+/+}$ (A, D, J), *Fmod*$^{-/-}$;*Lum*$^{+/+}$ (B, E, F, K), *Fmod*$^{-/-}$;*Lum*$^{+/-}$ (G, H, L) and *Fmod*$^{-/-}$;*Lum*$^{-/-}$ (C, I) hearts from 1.5 month to 5 months old. PV- pulmonary valve; RV- right ventricle; Ao- aorta, LV- left ventricle; LA- left atrium. Solid arrows- ectopic tissue; open arrows- extra cusp/leaflet-like extensions. Scale bars: A= 280μm applies to B-I; J= 700μm applies to K and L. Movies have been added to demonstrate

Author Manuscript Author Manuscript Author Manuscript Author Manuscript

the three-dimensional changes that correspond to the aortic malformation shown in the *Fmod*$^{-/-}$;*Lum*$^{+/+}$ heart in F and the *Fmod*$^{-/-}$;*Lum*$^{+/-}$ heart shown in panel K.

Author Manuscript Author Manuscript Author Manuscript Author Manuscript

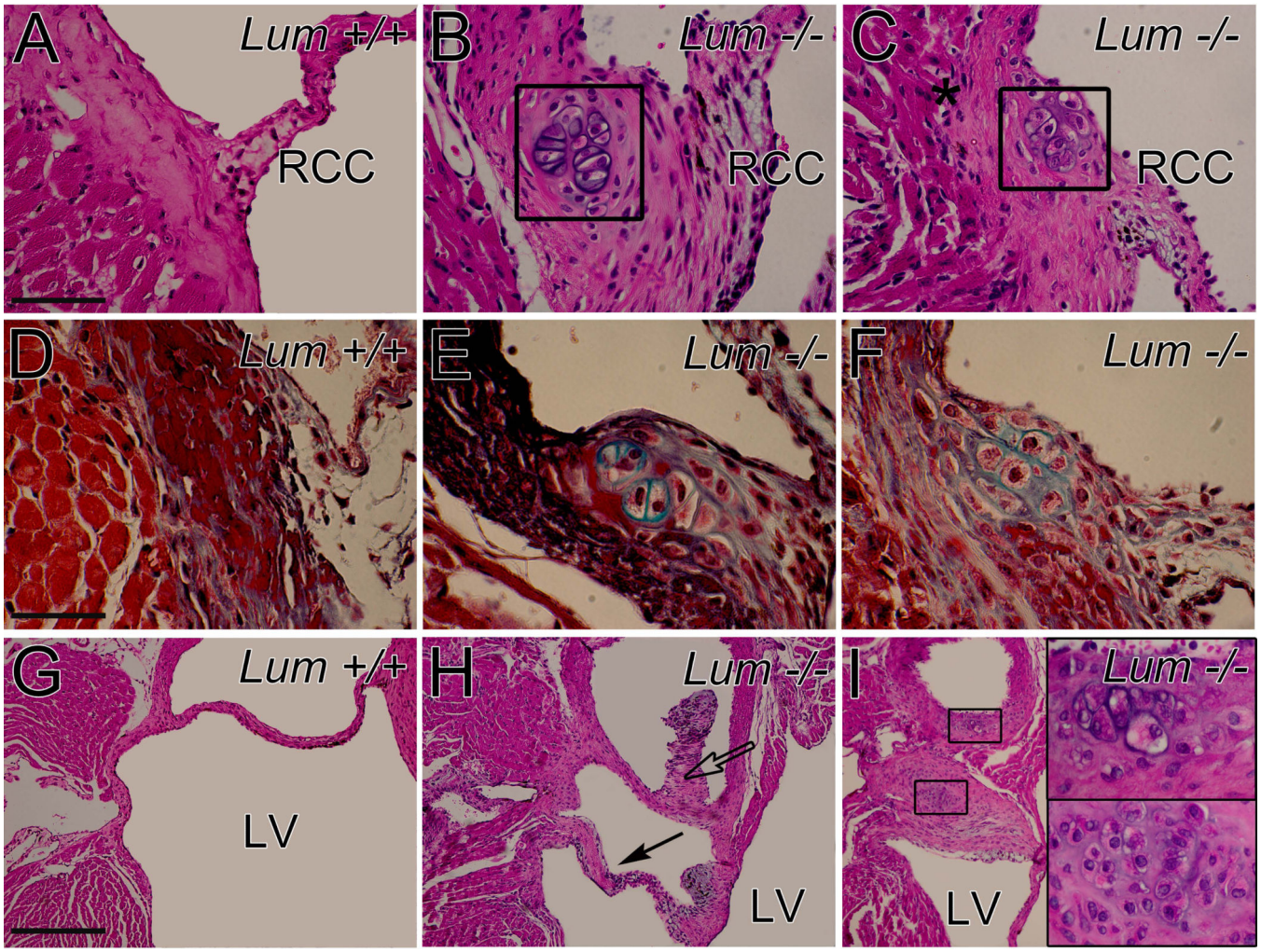


**Fig. 5. Mice deficient in lumican showed cartilage-like nodules in the annulus and adjacent to aortic valve cusps**

Hematoxylin and eosin stained sections of the anchor region of the aortic valve right coronary cusp (RCC) in *Lum*$^{+/+}$ (A) and *Lum*$^{-/-}$ (B, C) adult hearts. Movat's pentachrome stained sections (D-F) highlight cartilage-like nodules (green) in the *Lum*$^{-/-}$ (E, F) hearts. Hematoxylin and eosin stained sections of the aortic valve non coronary cusp (NCC; G, H); boxes (I) show magnified lacunae (cartilage-like regions). Solid arrow- abnormal valve extension; open arrow- extra tissue of the NCC; Ao- aorta; LV- left ventricle. Scale bars: A= 70 μm applies to B, C; D= 45μm applies to E and F, insets in I; G= 280μm applies to H and I.

Author Manuscript Author Manuscript Author Manuscript Author Manuscript

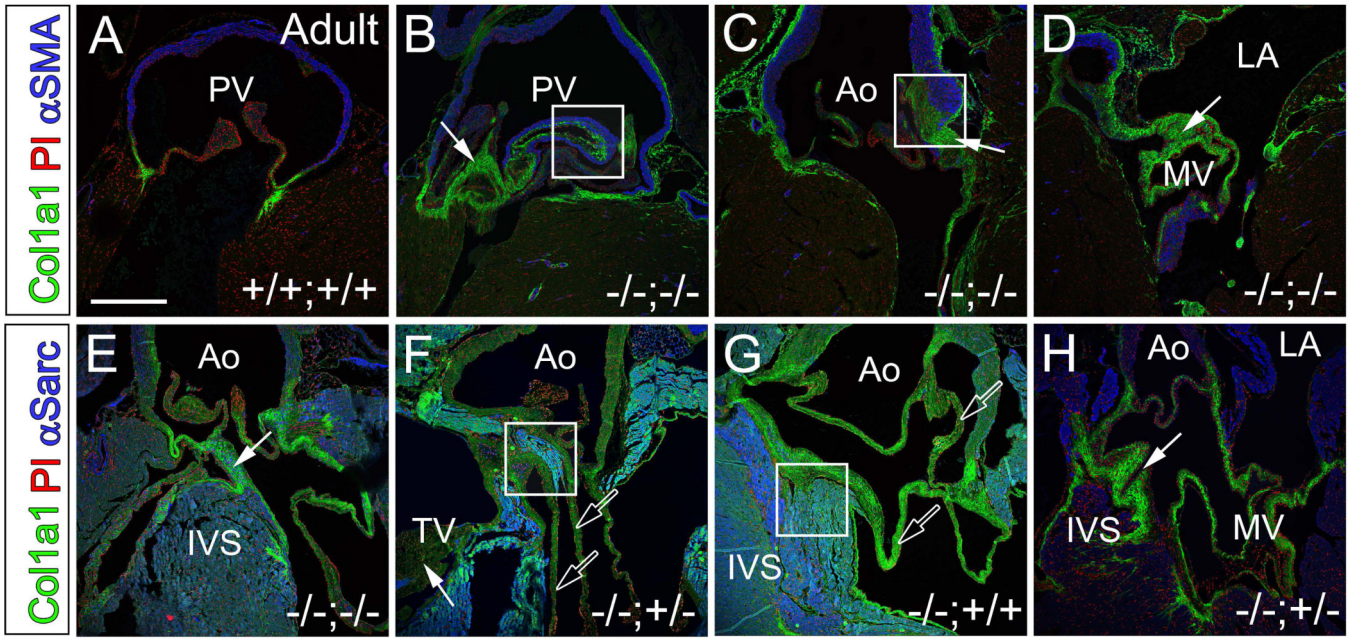


**Fig. 6. Col1a1 immunolocalized to ectopic valve-like tissue in *Fmod*$^{-/-}$;*Lum*$^{+/+}$, *Fmod*$^{-/-}$;*Lum*$^{+/-}$ and *Fmod*$^{-/-}$;*Lum*$^{-/-}$ adult hearts**

Immunolocalization of Col1a1 in the pulmonary valve (green, A-B), aortic valve (C, E, F, G, H) and mitral valve (D, H) in hearts from 1.5 to 5 month old mice. Boxes highlight areas of ectopic muscle (blue, B, C, F, G). Solid arrows- valve anchor abnormalities; open arrows- ectopic valve leaflet-like extensions; PV- pulmonary valve; Ao- aorta; IVS- interventricular septum; TV- tricuspid valve. Red- propidium iodide (PI); blue- αSMA (A-D); αSarc (E-H). Scale bar: A= 400μm applies to B-H.

Author Manuscript Author Manuscript Author Manuscript Author Manuscript

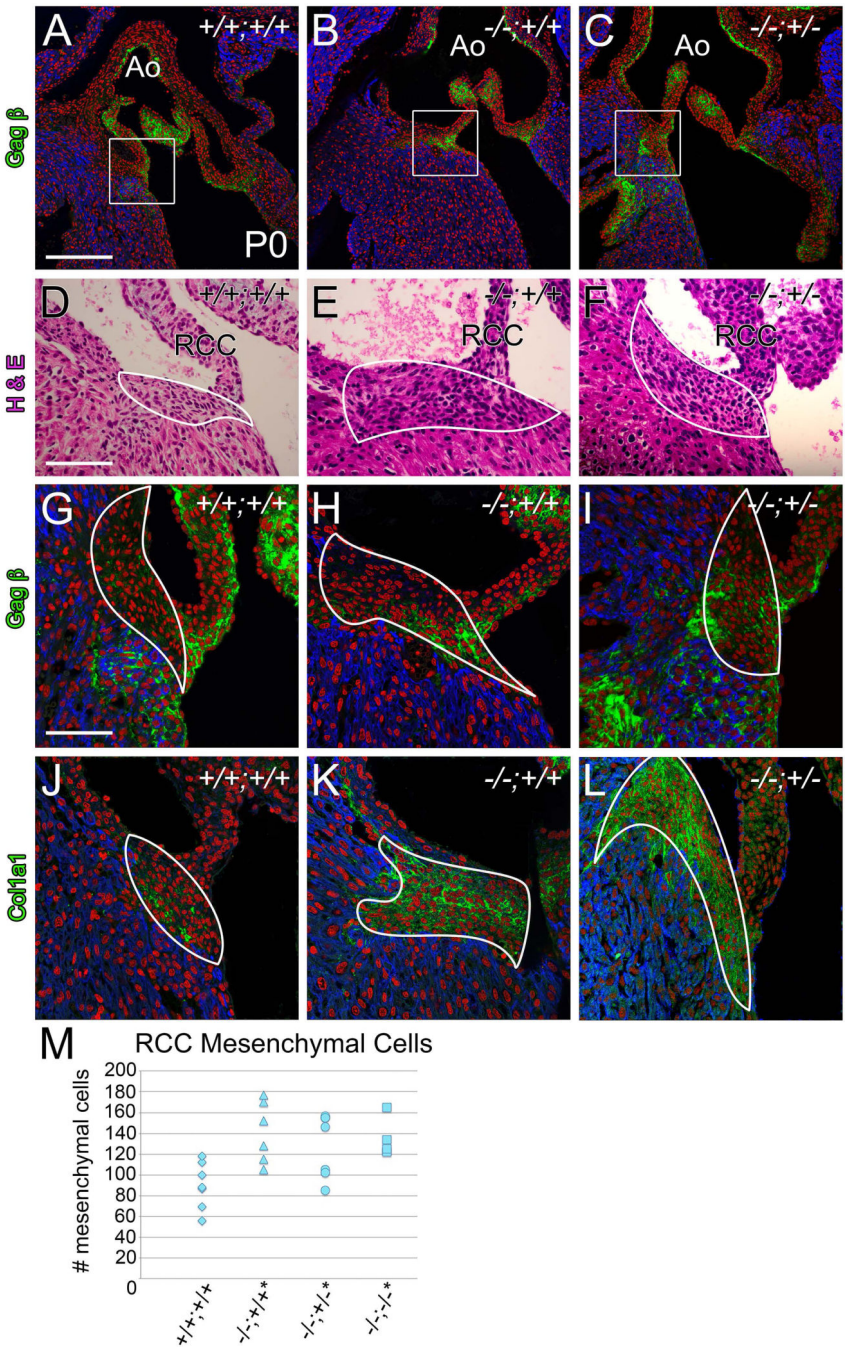


**Fig. 7. Postnatal day 0 *Fmod*$^{-/-}$;*Lum*$^{+/+}$ and *Fmod*$^{-/-}$;*Lum*$^{+/-}$ hearts exhibited an increase in mesenchymal cell number, at the attachment of the right coronary cusp (RCC)**

Immunohistochemistry of Vcan (GAGβ) in P0 aortic valve sections shown in panels A-C (green); boxes in A-C are magnified in (G-I). Hematoxylin and eosin stained sections of RCC mesenchyme are depicted and outlined (white, D-F). Immunolocalization of Col1a1 (green, J-L). Red- propidium iodide (PI); blue- αSarc; Ao- aorta. Scale bars: A= 200μm applies to B and C; D= 70 μm applies to E and F; G= 50μm and applies to H-L. Scatter plot in M shows mesenchymal cell counts of RCC mesenchyme in *Fmod*$^{+/+}$;*Lum*$^{+/+}$ (+/+;+/+, n=7) *Fmod*$^{-/-}$;*Lum*$^{+/+}$ (−/−;+/+, n=6; 50% penetrance, **P*<0.05), *Fmod*$^{-/-}$;*Lum*$^{+/-}$ (−/−;+/

Author Manuscript Author Manuscript Author Manuscript Author Manuscript

−, n=7; 57% penetrance, **P* <0.05) and *Fmod*$^{-/-}$;*Lum*$^{-/-}$ (−/−;−/−, n=4; 75% penetrance, **P* <0.05).

Author Manuscript Author Manuscript Author Manuscript Author Manuscript

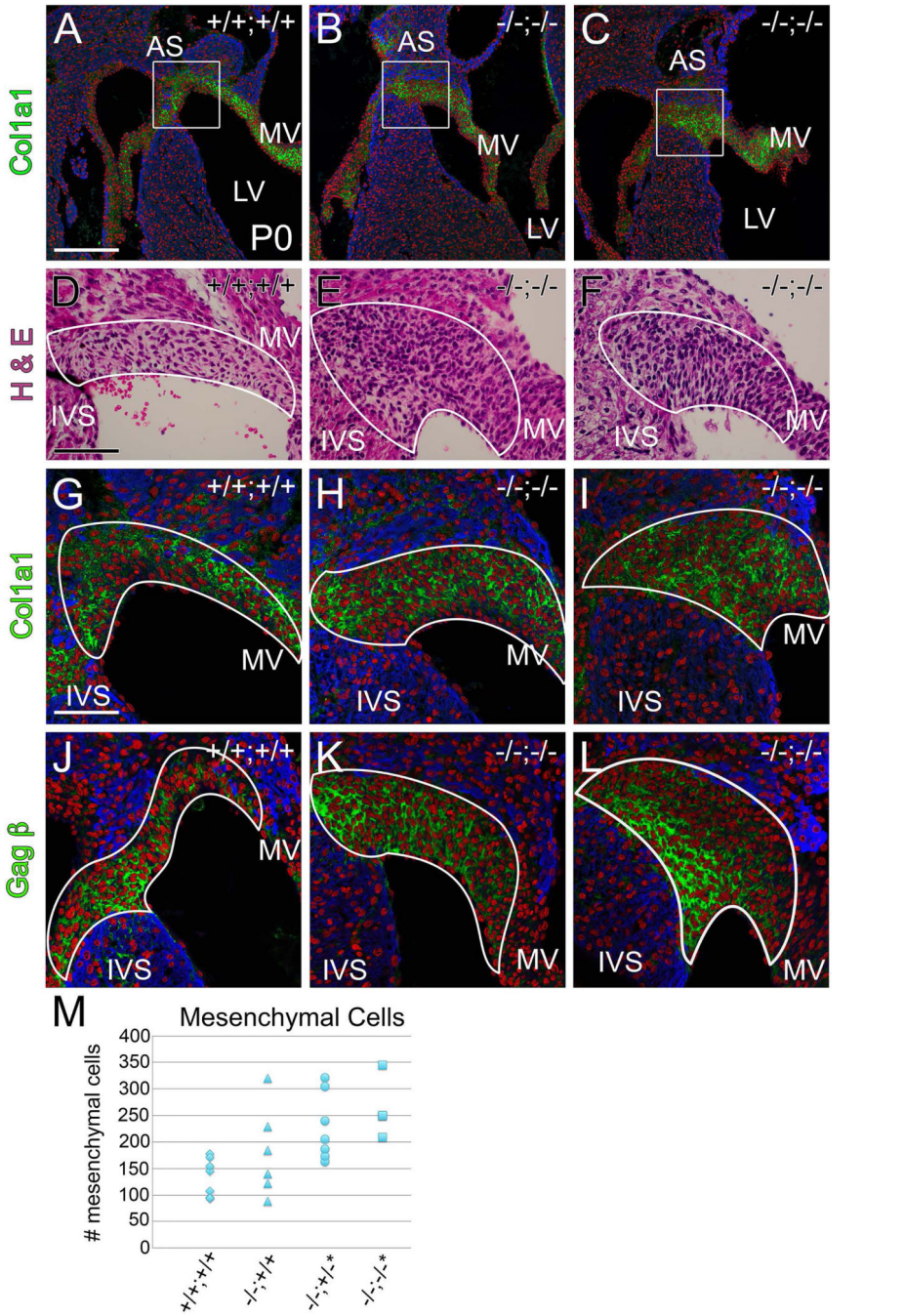


**Fig. 8. Mesenchymal cell number was increased at the juncture of the mitral valve leaflet with the interventricular septum at postnatal day 0 in the *Fmod*$^{-/-}$;*Lum*$^{+/-}$ and *Fmod*$^{-/-}$;*Lum*$^{-/-}$ hearts**

Histological sections from *Fmod*$^{+/+}$;*Lum*$^{+/+}$ (A, D, G, J,) and *Fmod*$^{-/-}$;*Lum*$^{-/-}$ (B, C, E, F, H, I, K, L) hearts are shown. Immunohistochemistry of Col1a1 in P0 hearts (green, AC; G-I) is depicted; boxes in A-C are magnified in G-I. Hematoxylin and eosin stained sections at the juncture of the interventricular septum (IVS) and mitral valve (MV) are shown (D-F); immunolocalization of Vcan (GAGβ) (green, J-L). IVS- Interventricular septum; AS- Atrial septum; LV- left ventricle. Red- propidium iodide (PI); blue- αSarc. Scale bars: A= 200μm

applies to B and C; D=70 μm applies to E and F; G= 50μm and applies to H-L. Scatter plot in M shows mesenchymal cell counts of IVS/MV mesenchyme in *Fmod*$^{+/+}$;*Lum*$^{+/+}$ (+/+;+/+, n=7) *Fmod*$^{-/-}$;*Lum*$^{+/+}$ (−/−;+/+, n=6; 50% penetrance), *Fmod*$^{-/-}$;*Lum*$^{+/-}$ (−/−;+/−, n=7; 57% penetrance **P* < 0.02) and *Fmod*$^{-/-}$;*Lum*$^{-/-}$ (−/−;−/−, n=4; 100% penetrance,**P* < 0.002).

Author Manuscript Author Manuscript Author Manuscript Author Manuscript

Author Manuscript Author Manuscript Author Manuscript Author Manuscript

## Table 1

Cardiac valve anomalies were found in 1-4 month old FMOD and LUM deficient mice. The percentage of cardiac valve related anomalies are presented. Valve anchor anomalies i.e. MTLJ-myotendinous junction-like region are shown for the various genotypes. The bolded percentages of the *Fmod−/−;Lum+/+*, *Fmod+/+;Lum −/−*, *Fmod−/−;Lum+/−* and *Fmod−/−;Lum−/−*, indicate where malformations were at least double the percentage observed in WT (*Fmod+/+;Lum+/+*). For several malformations (valve anchors, AV and MV) the penetrance of the *Fmod−/−;Lum+/−* phenotype was higher than in hearts from single mutants (*Fmod−/−;Lum +/+* and *Fmod+/+;Lum−/−*); in this case the percentile was bolded and underlined.

| **Age: 1 - 4 Months** | ***Fmod* +/+ *Lum* +/+ N=23** | ***Fmod* −/− *Lum* +/+ N=16** | ***Fmod*+/+ *Lum* −/− N=15** | ***Fmod* −/− *Lum* +/− N=13** | ***Fmod* −/− *Lum* −/− N=3** |
|---|---|---|---|---|---|
| **Valve Anchor Anomalies (MTJL)** | 0% | **44%** | **27%** | **77%** | **100%** |
| **Pulmonary Valve Anomalies** | 17% | **53%** | 7% | **40%** | 66% |
| Bicuspid | 0% | **34%** | 0% | **31%** | 66% |
| **Aortic Valve Anomalies** | 26% | 20% | 20% | **46%** | **100%** |
| Bicuspid | 22% | 0% | 13% | **31%** | **100%** |
| **Mitral Valve Anomalies** | 0% | **43%** | **13%** | **77%** | **66%** |
| **Tricuspid Valve Anomalies** | 0% | 13% | 7% | **23%** | **66%** |

Author Manuscript Author Manuscript Author Manuscript Author Manuscript



**Table 2**

Postnatal day 0 and embryonic day 17 hearts from FMOD and LUM deficient mice were examined for anomalies in mesenchyme associated with the right coronary cusp and at the junction of the mitral valve leaflet and the mesenchymal cap of the interventricular septum. Bold percentages represent genotypes that showed anomalies at frequencies more than double wild type penetrance. Underlined percentages denote double-deficient mice that showed a higher penetrance than the single gene deletions. RCC-right coronary cusp; MV-mitral valve; IVS-interventricular septum. Note that there were no anomalies detected in the embryonic day 17 samples of the *Fmod−/−;Lum+/+* and *Fmod+/+;Lum−/−*; and *Fmod−/−;Lum−/−* in the RCC or the MV anchor regions.

| **Postnatal Day 0** | ***Fmod*+/+; *Lum*+/+ N=7** | ***Fmod*−/−; *Lum*+/+ N=6** | ***Fmod*+/+; *Lum* −/− N=7** | ***Fmod*−/−; *Lum*+/− N=7** | ***Fmod*−/−; *Lum*−/− N=4** |
|---|---|---|---|---|---|
| **RCC Valve Anchor Mesenchyme Anomalies** | 0% | **50%** | **28%** | **57%** | **75%** |
| **Posterior MV Leaflet/IVS Mesenchymal Cap Anomalies** | 0% | **50%** | **86%** | **57%** | **100%** |

| **Embryonic Day 17** | ***Fmod*+/+; *Lum*+/+ N=3** | ***Fmod*−/−; *Lum*+/+ N=3** | ***Fmod*+/+; *Lum* −/− N=6** | ***Fmod*−/−; *Lum*+/− N=6** | ***Fmod*−/−; *Lum*−/− N=3** |
|---|---|---|---|---|---|
| **RCC Valve Anchor Mesenchyme Anomalies** | 0% | 0% | 0% | 0% | 0% |
| **Posterior MV Leaflet/IVS Mesenchymal Cap Anomalies** | 0% | 0% | 0% | 0% | 0% |